Experimental and Theoretical Investigation of High-Power Laser Ionization and Dissociation of Methane[†]

M. Sharifi,[‡] F. Kong,[§] S. L. Chin,[‡] H. Mineo,*,[#] Y. Dyakov,[#] A. M. Mebel,[⊥] S. D. Chao,[∥] M. Hayashi,[▽] and S. H. Lin[#,○]

Department of Physics, Engineering Physics and Optics, Laval University, Quebec City, Quebec, GIK 7P4, Canada, Institute of Chemistry, Chinese Academy of Science, Beijing 100080, People's Republic of China, Institute of Atomic and Molecular Science, Academia Sinica, P.O. Box 23-166, Taipei, Taiwan, Department of Chemistry and Biochemistry, Florida International University, Miami, Florida 33199, Institute of Applied Mechanics, National Taiwan University, Taipei 106, Taiwan, Center for Condensed Matter Sciences, National Taiwan University, Taipei 106, Taiwan, and Department of Applied Chemistry, National Chiao-Tung University, Hsin-chu, Taiwan

Received: May 25, 2007; In Final Form: July 30, 2007

The main purpose of this paper is to report the high-power laser ionization−dissociation of CH_4 at various femtosecond (fs) laser intensities (from 1×10^{14} W/cm² to 2×10^{15} W/cm²) with a laser pulse duration of 48 fs. The generalized molecular Keldysh theory has been applied to calculate the ionization yields for CH_4^+ and CH_4^{++}. Outside the influence of the fs intense laser, we propose to calculate the mass spectra due to the decomposition of CH_4^+ and CH_4^{++}, using the Rice−Ramsperger−Kassel−Marcus (RRKM) theory. The agreement between the experimental mass spectra and calculated mass spectra seems to be reasonable.

1. Introduction

The earliest experiment on the fragmentation of energy-selective methane (CH_4) ions was that of von Koch in 1964,[1] in which the ions were generated by charge exchange. Later, the photoelectron photoion coincidence (PEPICO) techniques[2,3]—particularly, the form that uses zero energy or threshold electrons (TREPICO)—has been used to examine the fragmentation of energy-selective CH_4 ions.[4−6] The ground-state case has been studied in detail, and the Rice−Ramsperger−Kassel−Marcus (RRKM) theory has been used successfully to explain the experimental results.[4]

Recently, the application of an intense ultrashort laser to ionize and dissociate molecules has attracted considerable attention.[7−14] The conventional knowledge of the high-power laser ionization−dissociation of molecules is that the molecule is first ionized in the intense laser field, followed by fragmentation of the molecular ions.[7−18]

In this paper, we shall report the experimental results of the high-power laser ionization−dissociation of CH_4 performed using the 800-nm laser with a pulse duration of 48 fs and with a laser intensity that varies from 1.5×10^{14} W/cm² to 1.9×10^{15} W/cm². Depending on the laser intensity, both CH_4^+ and CH_4^{++} and their fragmented daughter ions can be observed.

Recently, the fragmentation pattern of CH_4 was experimen-tally studied at an intensity of $\sim 10^{14}$ W/cm², with the laser duration varying from 8 fs to 110 fs. For the case in which the laser duration was 8 fs, only the primarily fragmental CH_3^+ ion was observed, in addition to the parent CH_4^+ ion. When the laser duration was increased to 30 fs, CH_2^+ and H^+ began to appear, and when the laser duration reached 110 fs, some doubly charged ions were also observed, in addition to the abundant singly charged ions.[19,20] The field-assisted dissociation (FAD) model and quasi-classical trajectory (QCD) calculation were applied to predict the dissociation probability of CH_4^+.[19−21] The calculated probability was corrected with the molecular orientation effect and the spatial distribution of laser intensity. The modified results indicated that the dissociation would require at least 23 fs and was saturated with long pulse widths ($\sim$100 fs).

The present paper is organized as follows. In section 2, the experimental setup and experimental results will be presented, which will be followed by the theoretical treatment of the high-power laser ionization of CH_4 (section 3). We will discuss the calculation of the dissociation patterns of CH_4^+ and CH_4^{++} in section 4. Discussion and the conclusion will be presented in section 5.

2. Experiment

2.1. Experimental Setup. Figure 1a schematically shows the experimental setup. We have used a commercial laser system (built by Spectra Physics) that consists of a Ti:sapphire oscillator (Tsunami), followed by a regenerative amplifier (spitfire). The 10 Hz seed from the spitfire passes through a two-pass Ti:sapphire amplifier and compressor. The laser pulses have a central wavelength of 800 nm and the compressed pulse has a pulse duration of 48 fs (fwhm), as measured by a single-shot auto-correlator (made by Positive Light), and the maximum output energy is 12 mJ/pulse.

* Author to whom correspondence should be addressed. Tel.: 886 2 2364 4261. Fax: 886 2 2362 0200. E-mail: mineo@gate.sinica.edu.tw.
  † Part of the "Sheng Hsien Lin Festschrift".
  ‡ Department of Physics, Engineering Physics and Optics, Laval University.
 § Institute of Chemistry, Chinese Academy of Science.
  # Institute of Atomic and Molecular Science, Academia Sinica.
 ⊥ Department of Chemistry and Biochemistry, Florida International University.
  ∥ Institute of Applied Mechanics, National Taiwan University.
  ▽ Center for Condensed Matter Sciences, National Taiwan University.
  ○ Department of Applied Chemistry, National Chiao-Tung University.
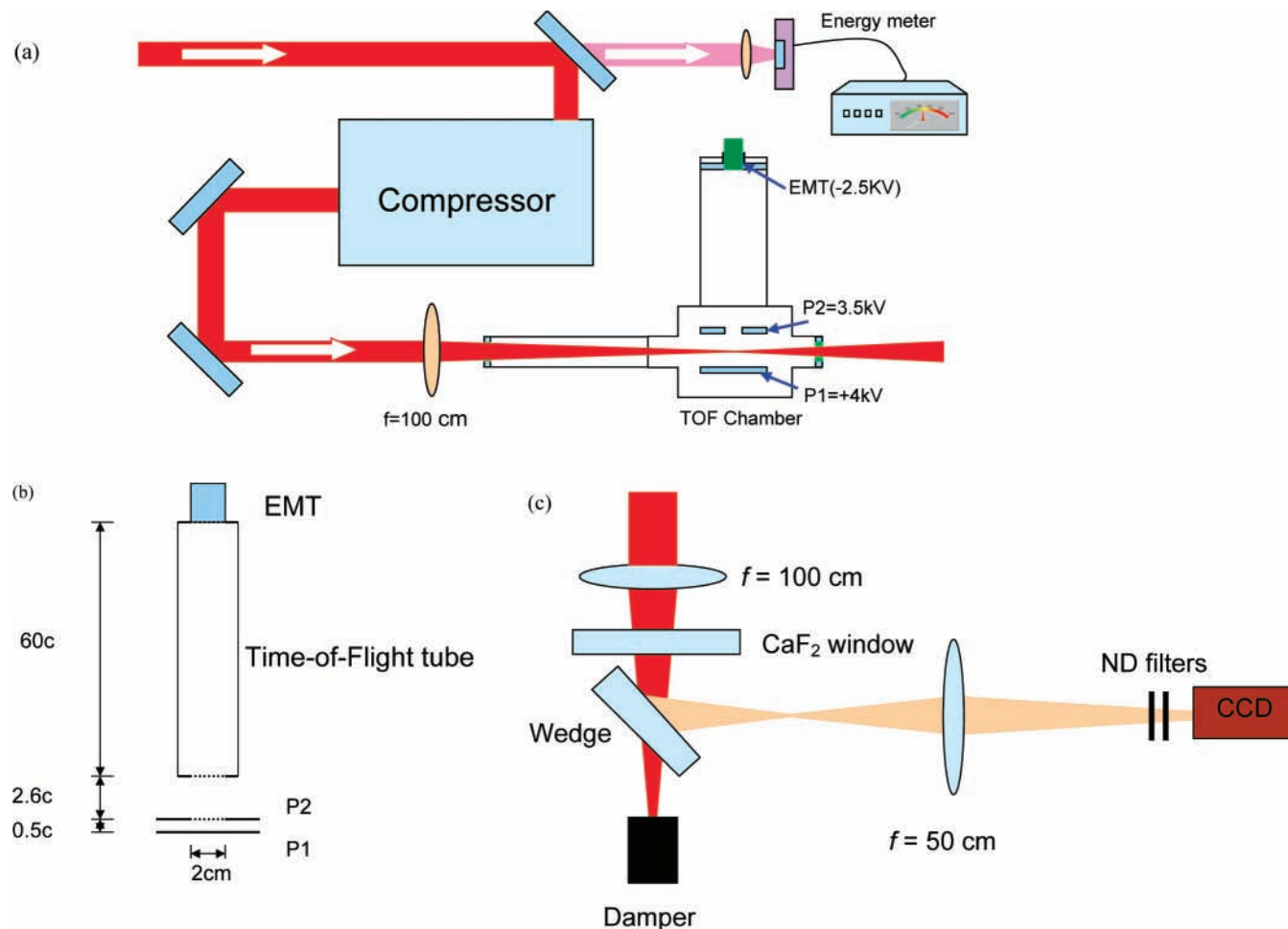
Figure 1. Experimental setup for (a) laser and time-of-flight (TOF) mass spectrometer, (b) ion detection, and (c) measurement of the focal point.
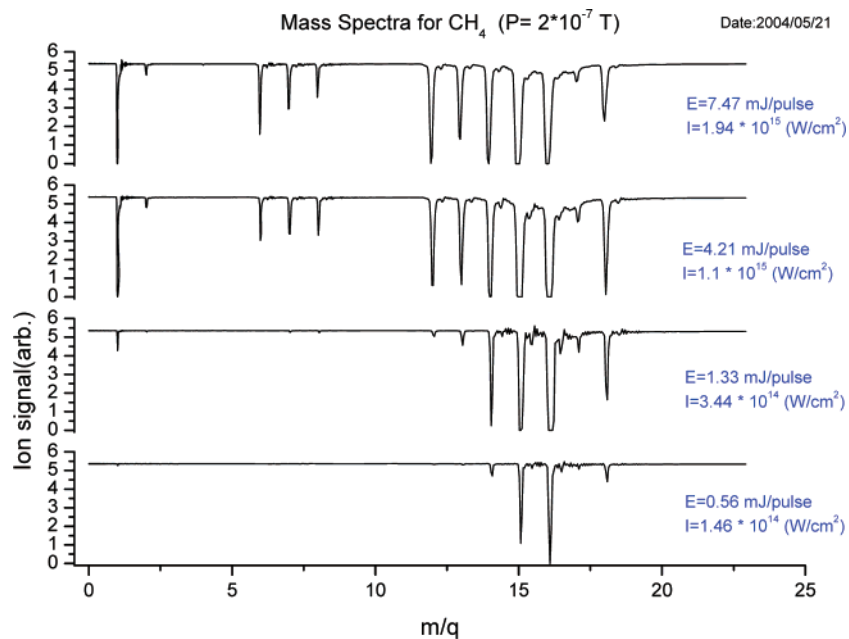
Figure 2. Some mass spectrum of CH_4 at different intensities.

The linearly polarized laser pulses are focused into the interaction chamber using a $f = 100$ cm focusing lens. A pyroelectric energy meter (Molectron EPM 1000) is placed behind the last mirror in the laser path before the compressor, to monitor the laser energy by detecting the leak from the mirror.

CH_4 molecules are injected into the high-vacuum chamber of the time-of-flight (TOF) mass spectrometer through a variable-leak valve. The background pressure was 5×10^{-9} Torr, whereas the pressure of CH_4 molecules was set at different pressures, from 1×10^{-8} Torr to 5×10^{-6} Torr, depending on the intensity used. Higher pressures are used at lower intensities,
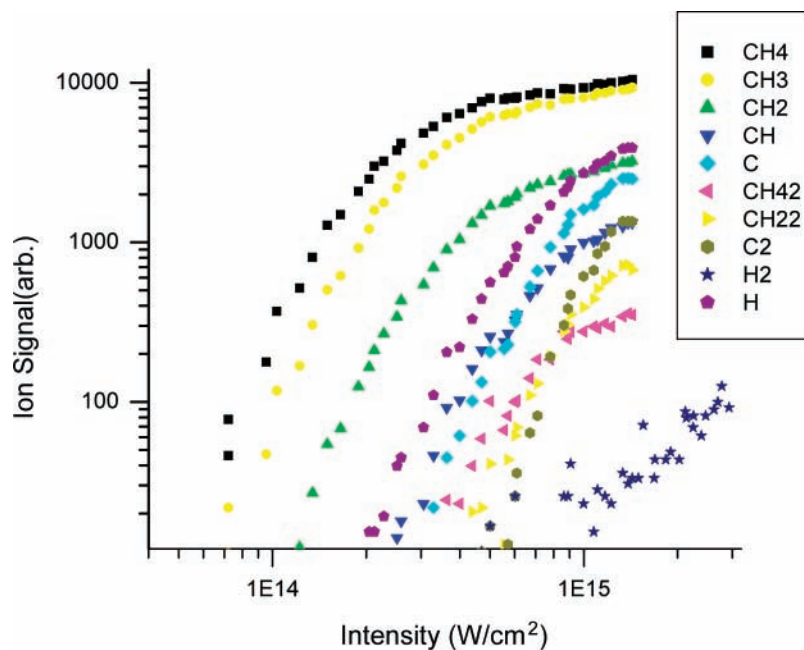
Figure 3. Ion signal versus intensity for the CH_4 parent ion and fragments of CH_4.
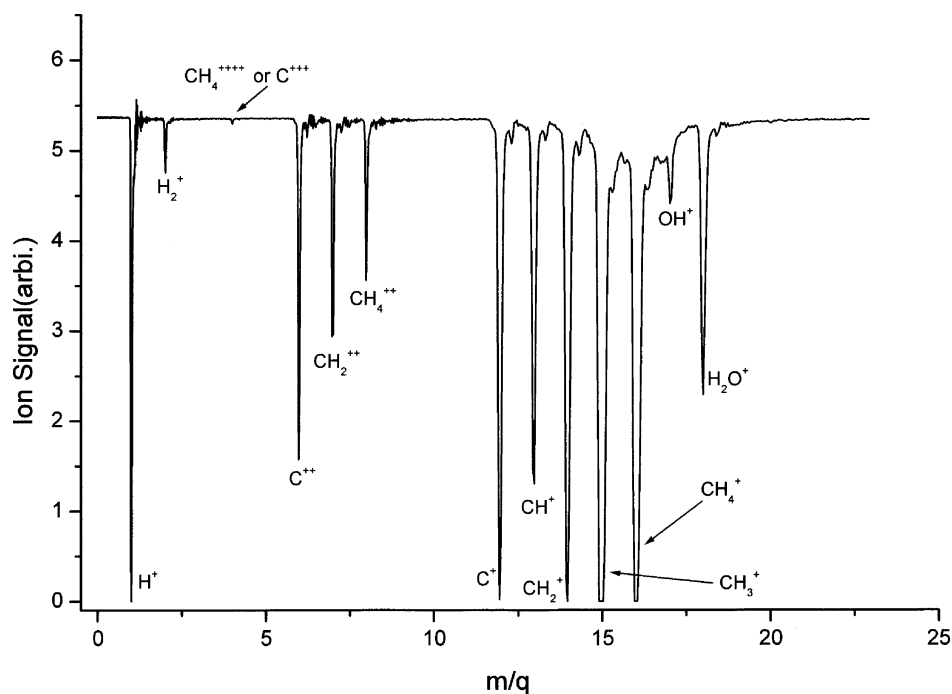

Figure 4. Mass spectra of CH_4 at a pressure of $P = 2 \times 10^{-7}$ Torr and intensity of 1.9×10^{15} W/cm^2.

to avoid the saturation of the ion detector (electron multiplier tube (EMT)). The CH_4 molecules interact with the laser pulses, and the parent and fragment ions are accelerated by a static field of 500 V/cm toward the ion detector through an opening 2 cm in diameter, followed by a field-free flight path of 60 cm. As shown in Figure 1b, there are two openings. One is located at the site marked P2 in Figure 1 and one is located at the entrance of the TOF tube. A fine metallic mesh is welded at both openings, to ensure a uniform electric field. The transmission of the mesh is ~99%. An EMT (Thorn EMI electron tube, type 105 EM) with a detection area of diameter $\varphi = 21.6$ mm was used to detect the ions. The signals at different laser energies were recorded using a 500 MHz oscilloscope (Tektronix TDS 504A). Measurements of the focal spot area and the averaged

laser intensity have been performed outside the chamber, as shown in Figure 1c.

For the focal spot measurement, the focus is imaged onto a charge-coupled device (CCD) camera (Cohu 4810) after the wedge. In this measurement, low pulsed energy is used while the wedge with good optical surface quality further reduces the energy of the pulse at the focus in air, so that ionization is avoided. The laser intensity at the focus was calculated from the laser pulse energy, the pulse duration, and the measured focal area.

2.2. Experimental Results. Figure 2 shows the evolution of mass spectrum of CH_4 at different laser intensities. Some of the ions peaks are saturated (flat-top peaks), to enhance the weaker peaks for inspection. In the quantitative measurement

9408 *J. Phys. Chem. A, Vol. 111, No. 38, 2007*

Sharifi et al.

(see discussion below), such saturation is avoided. Figure 3 shows the ion signal versus intensity for parent ion and fragments of CH_4, and a particular case of mass spectra at the laser intensity of 1.9×10^{15} W/cm^2 is shown in Figure 4. The assignment of the mass spectra for the ionization−dissociation of CH_4 is shown in Figure 4; from this figure, we can see that the impurity ions (such as H_2O^+ and OH^+) can be observed.

3. Theoretical Treatments of High-Power Laser Ionization of Molecules

In this section, we will show how to compute the molecular cations using the generalized Keldysh theory,[22] which is developed from the original Keldysh theory[23] by combining the molecular orbital (MO) theory and the Born−Oppenheimer (BO) approximation. The wave function for the electronic ground state of the molecules and molecular cations are obtained from ab initio calculations. For the ionized state, the ionized electron wave function is described by the Volkov continuum state,

$$\psi_{\vec{p}}(\vec{r},t) = \exp\left\{i\left[(\vec{p} - \vec{e}A(t))\cdot\vec{r} - \frac{1}{2m_e}\int_{-\infty}^{t} dt'(\vec{p} - e\vec{A}(t'))^2\right]\right\} \quad (3-1)$$

where e is the charge of the electron ($e = -1$), $\vec{p}$ is the momentum of the ionized electron, and, under the dipole approximation, the vector potential $\vec{A}(t)$ is given by $\vec{A}(t) = -\vec{F}\sin(\omega t)/\omega$ for the linearly polarized laser field $\vec{F}(t) = \vec{F}\cos(\omega t)$.

The total electronic wave function of the molecule and molecular cation is expressed as

$$\Psi_M(\vec{r}_1,...,\vec{r}_{N_e},t) = \Psi_g(\vec{r}_1,...,\vec{r}_{N_e},t) + \int \frac{d^3p}{(2\pi)^3} c_{\vec{p}}(t)\Psi_{I,\vec{p}}(\vec{r}_1,...,\vec{r}_{N_e},t) \quad (3-2)$$

where N_e is the number of electrons and

$$c_{\vec{p}}(t) = -i\int_{-\infty}^{t} dt' \langle \Psi_{I,\vec{p}}(\vec{r}_1,...,\vec{r}_{N_e},t)|V_L(\vec{r}_1,...,\vec{r}_{N_e},t)|\Psi_g(\vec{r}_1,...,\vec{r}_{N_e},t) \rangle \quad (3-3)$$

with

$$V_L(\vec{r}_1,...,\vec{r}_{N_e},t) = -\sum_{i=1}^{N_e} e\vec{r}_i\cdot\vec{F}\cos(\omega t) \quad (3-4)$$

Therefore, by following the approach of Keldysh,[22−24] the ionization rate constant $k(\vec{F})$ can be written as

$$k(\vec{F}) = \sum_{j=1}^{d} \frac{2\pi S}{d}|c_j|^2 \int \frac{d^3p}{(2\pi)^3}|L_j(\vec{p})|^2$$
$$\sum_{N=-\infty}^{\infty} \delta\left(I_0 + U + \frac{p^2}{2m} - N\hbar\omega\right) \quad (3-5)$$

where c_j represents the coefficients of the linear combination of atomic orbitals (LCAO) MO, I_0 is the ionization potential of molecule, and U is the ponderomotive energy ($U = (eF)^2/(4m\omega^2)$). Here, d is the degeneracy of energy states, $S = \sqrt{2}$ for the closed shell, and $S = 1$ for the open shell. Using the analytical continuation to the complex plane,[24,25] $L_j(\vec{p})$ is given by

$$L_j(\vec{p}) = \frac{1}{2\pi}\int_C duV_j\left[\vec{p} + \left(\frac{e\vec{F}}{\omega}\right)u\right]\exp\left(\frac{ij(u)}{\omega}\right) \quad (3-6)$$

where

$$j(u) = N\omega\left(\frac{1}{i}\right)\log[iu + (-i\sqrt{u-1}\sqrt{u+1})] - \xi(-i\sqrt{u-1}\sqrt{u+1}) - Uu(-i\sqrt{u-1}\sqrt{u+1}) \quad (3-7)$$

Here we have

$$V_j(\vec{p}) = -K\left[\frac{\vec{F}\cdot\vec{p}(\vec{p})_j}{m(I_0 + p^2/(2m))^4} - \frac{(\vec{F})_j}{3(I_0 + p^2/(2m))^3}\right] \quad (3-8)$$

where

$$u = \sin(\omega t)$$
$$K = 96e\sqrt{\pi a^5 I_0^3}$$
$$\xi = e\vec{p}\cdot\frac{\vec{F}}{m\omega}$$

Note that $V_j(\vec{p} + e\vec{F}/\omega u)$ has two poles, at $u = u_+$ and $u = u_-$, where

$$u_+ = \gamma\left(\frac{p\cos\theta}{\sqrt{2mI_0}} + i\sqrt{1 + \frac{p^2\sin^2\theta}{2mI_0}}\right) = u_-^*$$

and γ is the Keldysh parameter, which is given as

$$\gamma = \frac{\omega\sqrt{2mI_0}}{|e|F}$$

There are some possible choices of contour C, and the details of the calculations for eq 3-6 are given in the work by Mineo et al.[24,25]

For the multi-ionization of molecules, we consider the following sequential ionization process:

$$M \xrightarrow{k_1} M^+ \xrightarrow{k_2} M^{2+}\cdots\xrightarrow{k_n} M^{n+} \quad (3-9)$$
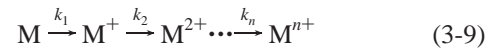
where k_i is the photoionization rate constant of the M^{i+} cation. The rate equation for eq 3-9 then can be written as

$$\frac{d}{dt}A(t) = -k_1A(t) \quad (3-10)$$

$$\frac{d}{dt}A^{i+}(t) = k_iA^{(i-1)+}(t) - k_{i+1}A^{i+}(t) \quad (3-11)$$

$$\frac{d}{dt}A^{n+}(t) = k_nA^{(n-1)+}(t) \quad (3-12)$$

with

$$A(t_0) = [M]_0, \quad A^{i+}(t_0) = 0 \quad (\text{for } i = 1, 2, ..., n) \quad (3-13)$$

where $A^{i+}(t)$ (for $i = 0, 1, ..., n$) represents the ionization yields of the molecule and molecular cations. Here, we remark that the photoionization rate constant is assumed to be almost independent of the laser time t during the pulse duration, which is checked in our previous work[18] by taking into account the laser pulse for the generalized Keldysh theory. In ref 18, the laser has a Gaussian shape,

$$\vec{F}(t)\cos(\omega t) = \vec{F}_0 \exp\left[-\frac{(4\ln 2)t^2}{(\Delta t_F)^2}\right]\cos(\omega t)$$

where the $\vec{F}_0$ is the peak amplitude and Δt_F is the full width at half-maximum (fwhm). We note that the pulse laser of a Gaussian shape is not used to calculate the rate constants.

As an outlook, it is very important to consider the time dependence of the pulse laser in solving the rate equations, because, in the actual ionizations, the single- and double-ionization processes will occur sequentially with some time difference, where the time dependence of the rate constant might have an important role.

By solving eqs 3-10 through 3-13, we obtain

$$A(t) = A_0 \exp[-k_1(t - t_0)] \qquad (3\text{-}14)$$

$$A^{i+}(t) = A_0\left(\prod_{j=1}^{i} k_j\right)\sum_{j=1}^{i+1}\frac{\exp[-k_j(t-t_0)]}{\prod_{\substack{l=1(\neq j)}}^{i+1}(k_l - k_j)}$$

$$(i = 1, 2, ..., n-1) \quad (3\text{-}15)$$

$$A^{n+}(t) = A_0\left(\prod_{j=1}^{n}k_j\right)\left\{\frac{1}{\prod_{j=1}^{n}k_j} - \sum_{j=1}^{n}\frac{\exp[-k_j(t-t_0)]}{k_j\prod_{\substack{l=1(\neq j)}}^{n}(k_l - k_j)}\right\} \quad (3\text{-}16)$$

It is also important to consider the spatial distribution of the laser pulse,[26] and, similar to ref 18, we assume that the laser has a Gaussian shape of the spatial distribution with a width ΔR, i.e.,

$$I(R) = I_0 \exp\left(-\frac{8R^2}{\Delta R^2}\right)$$

The ionization yield then is dependent on time and R (i.e., $A^{i+}(t,R)$), and we define the spatial averaged ionization yield as

$$\bar{A}^{i+}(t) = 4\pi\int_0^\infty dR\, R^2 A^{i+}(t,R) \qquad (3\text{-}17)$$

In Figure 5a, we have plotted the photoionization rate constants of the first and second ionizations for CH_4, using the generalized Keldysh theory. The ionization potentials of molecule and molecular cation are calculated using the GAUSSIAN03 package[27] and adopt the B3LYP method with STO-3G basis sets. The calculated ionization potentials are $I_0 = 12.08$ eV for the first ionization and $I_0 = 19.76$ eV for the second ionization. The laser wavelength is fixed at $\lambda = 800$ nm, and we set the time duration as $\Delta t_F = 48$ fs and the space width as $\Delta R = 30\ \mu$m.[26] If the laser intensity is $I < 10^{14}$ W/cm², the first ionization rate is much faster than the second one by a factor of more than 10^4; on the other hand, if the laser intensity is close to $I = 10^{15}$ W/cm², both the first and the second ionization rate constants are almost comparable. In Figure 5b,
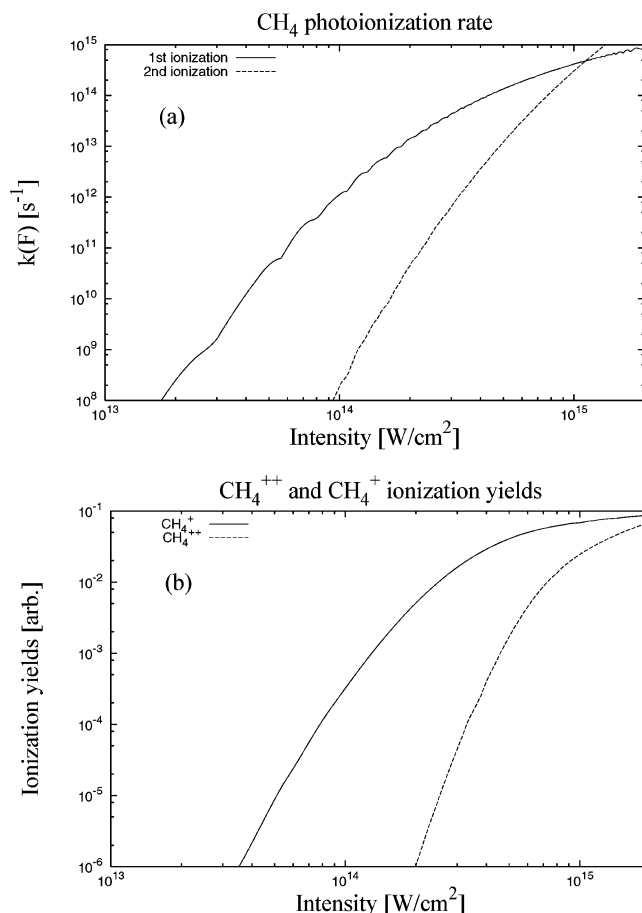
Figure 5. Plots of (a) the photoionization rate constants calculated by the generalized Keldysh theory for the first and second ionizations of CH_4, and (b) the ionization yields for CH_4^+ and CH_4^{++} (in arbitrary units).

we also find that, similar to the rate constants, if the laser intensity is $I < 10^{14}$ W/cm², the ionization yields of CH_4^+ are much larger than CH_4^{++} by a factor of more than 10^5, whereas if the laser intensity is close to $I = 10^{15}$ W/cm², the ionization yields of CH_4^+ and CH_4^{++} are comparable. This fact indicates that possible fragmentations of CH_4^{++} can happen for a laser intensity of $I \approx 10^{15}$ W/cm².

4. Theoretical Treatments of Dissociation of Molecular Ions

It is commonly believed that dissociation of a molecule under the influence of a high-power laser occurs via the initial ionization of the molecule in the intense laser field, followed by the fragmentation of molecular ions.

The dissociation of molecular ions induced by an intense femtosecond laser can proceed in two ways. Within the laser-pulse temporal duration and spatial distribution, the potential surfaces can be modified by the laser electric field, and if the laser intensity is strong enough, it can induce the ion dissociation during the laser duration. This type of dissociation is usually referred to as FAD[19−21] and occurs in the femtosecond range. The second type of ion dissociation occurs outside the temporal and spatial influence of the femtosecond laser pulse. In this case, the ions are hot and unstable; this type of dissociation for reasonably large-sized ions can be treated by a statistical theory−typically, the RRKM theory (or QET, quasi−equilib-
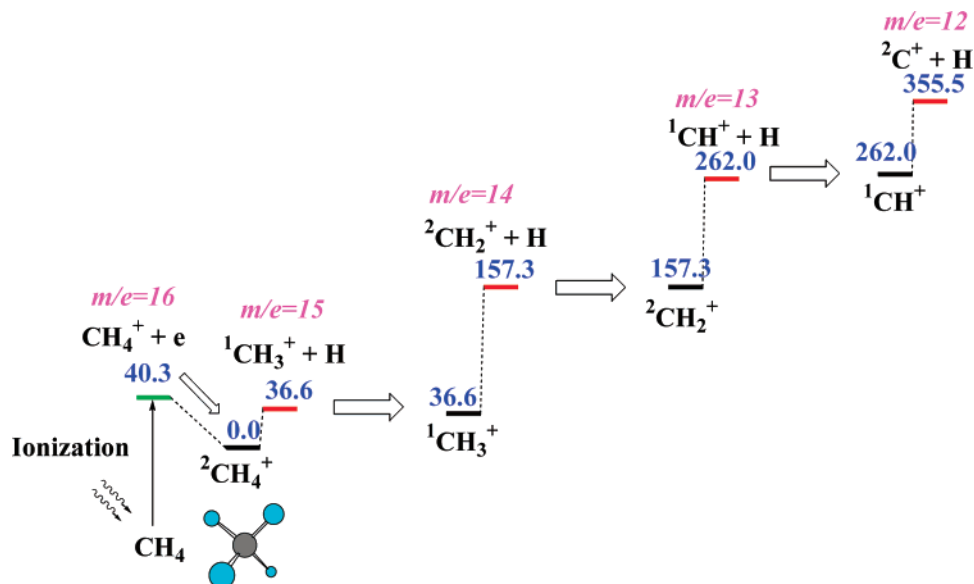
Figure 6. CH₄⁺ dissociation. (All energies are given in units of kcal/mol.)

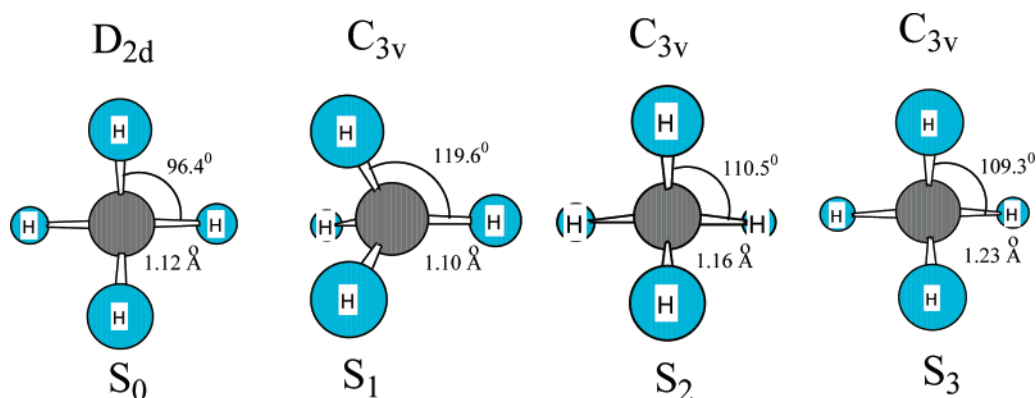**Figure 7.** Geometry of the CH₄⁺ ion in the ground and excited states.

rium theory). According to the RRKM theory, the unimolecular dissociation rate constant $k(E)$ can be expressed as[28−30]

$$k(E) = \frac{1}{h}\left(\frac{W^{\ddagger}(E - E_0^{\ddagger})}{\rho(E)}\right)$$ (4-1)

where $W^{\ddagger}(E - E_0^{\ddagger})$ and $\rho(E)$ denote the total number of states for the activated complex with activation energy $E_0^{\ddagger}$ and the density of states for the reactant with energy E, respectively. Application of the RRKM theory to the dissociation of CH₄ ions will be described in the following discussion.
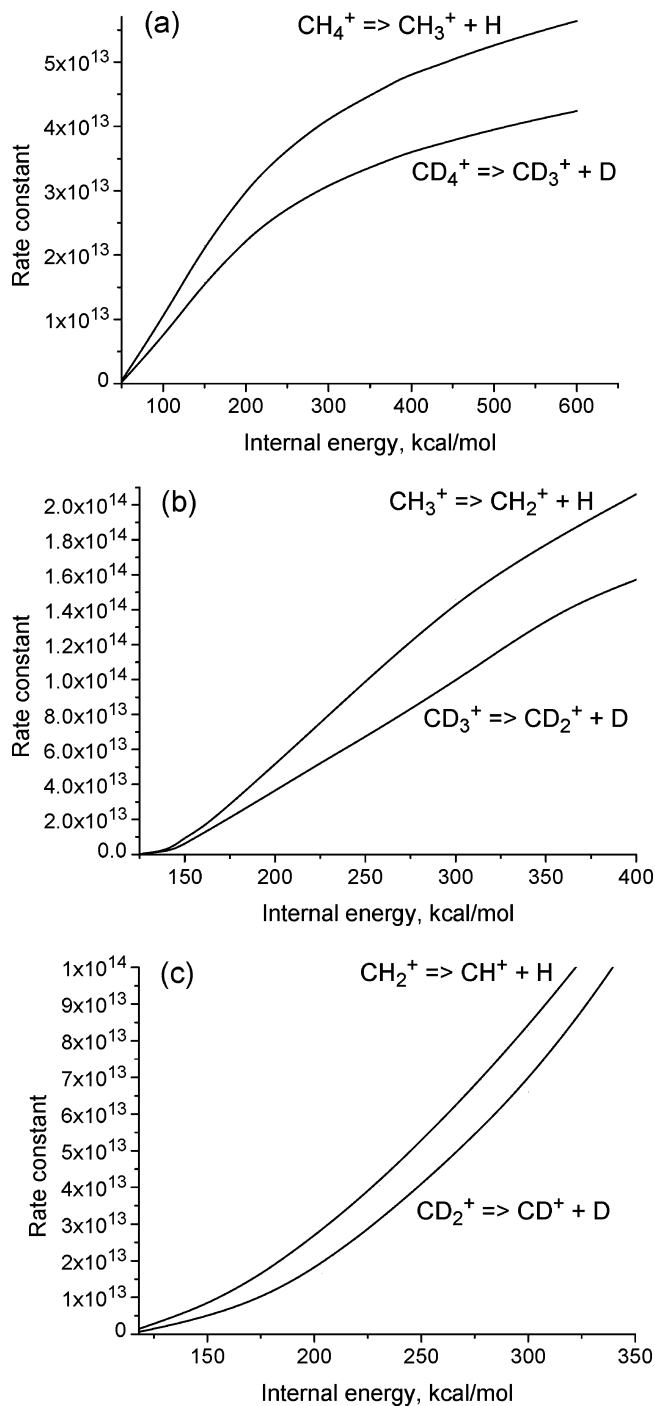
To investigate the dissociation mechanism of methane ions, ab initio quantum chemical calculations of potential energy surfaces were performed for the ground and excited states of CH₄⁺ and CH₄⁺⁺ ions and some of their fragments. Geometry optimizations for the ground state were performed using the B3LYP/cc-pVQZ method. After the geometry optimization, the energies of ions were refined by the CCSD(T)/cc-pVQZ ab initio calculations. The zero-point energy (ZPE) corrections to the total CCSD(T)/cc-pVQZ energies were computed using B3LYP/cc-pVQZ frequencies without scaling. Geometries and energies of excited states of CH₄ and CH₄⁺ were calculated at the CASSCF /6-31+G* level, where nine active orbitals were occupied by eight and seven electrons for the CH₄ and CH₄⁺ ions, respectively. To avoid any restrictions in the geometries of the transition states and intermediates, we did not use symmetry of the molecules in the excited-state calculations. All ab initio

calculations were performed using the GAUSSIAN 03[27] and MOLPRO 2002[31] packages. To compute the dissociation rate constants of the ions, the RRKM and microcanonical variational transition-state theories[28−30] have been applied. B3LYP/cc-pVQZ frequencies for all intermediates and transition states were used to perform the RRKM calculations.

4.1. CH₄⁺ Dissociation. The multistep dissociation scheme for the CH₄⁺ ion is presented in Figure 6. The following reactions occur without distinct transition states:

$$CH_4^+ \rightarrow CH_3^+ + H$$ (4-2a)

$$CH_3^+ \rightarrow CH_2^+ + H$$ (4-2b)

$$CH_2^+ \rightarrow CH^+ + H$$ (4-2c)

$$CH^+ \rightarrow C^+ + H$$ (4-2d)

In addition, the dissociation rate constant for these reaction channels can be computed by the variational TST theory. Because of the extremely short duration time of the laser pulses, we suppose that the secondary photon absorption by the reaction products is unlikely. Therefore, the appearance of the CH₃⁺, CH₂⁺, CH⁺, and C⁺ ions is dependent on the available internal energy of the initial CH₄ ions. Because of the significant difference between the equilibrium geometries of CH₄ and CH₄⁺ in the ground electronic state (i.e., the Frank−Condon effect), ionization of the CH₄ molecule, followed by geometry relax-

Figure 8. Singly charged ions dissociation rate constants versus available internal energy of the fragments: (a) $CH_4^+ \rightarrow CH_3^+ + H$ and $CD_4^+ \rightarrow CD_3^+ + D$, (b) $CH_3^+ \rightarrow CH_2^+ + H$ and $CD_3^+ \rightarrow CD_2^+ + D$, and (c) $CH_2^+ \rightarrow CH^+ + H$ and $CD_2^+ \rightarrow CD^+ + D$.

TABLE 1: Excitation Energy of the CH_4^+ Ion and the Internal Energy That Could Be Accumulated by CH_4^+ after Relaxation from an Excited State, Because of the Difference in the Geometry of the Excited and Ground States (Distortion Energy)

excited state	vertical excitation energy (eV)	distortion energy (kcal/mol)
S1	4.4	19.3
S2	5.3	25.1
S3	10.1	38.6
S4	11.4	
S5	13.1	

the ground electronic state of CH_4^+. All these excited states have C_{3v} symmetry. The first and second excited states are the result of electron transitions from a doubly occupied orbital to the singly occupied HOMO orbital of CH_4^+. Therefore, the geometry of these excited states is similar to the tetrahedron shape of the neutral CH_4 molecule, except that one of the C−H bonds is elongated in S_2 and S_3, whereas in S_1, the HCH′ angle involving the H′ atom on the C_3 axis increases to 119.6°. The higher excited states are the result of electronic transitions from doubly occupied orbitals to the lowest unoccupied orbital of CH_4^+. The geometry of these excited states is similar to the geometry of the ground triplet state. States S_4 and S_5 are unstable and rapidly decompose to form a H atom and a CH_3^+ ion.

It is necessary to estimate the amount of internal energy of various ions in the reactions shown in eq 4-2 to predict the mass spectra. Dissociation of CH_4^+ occurs if the energy of vibration along the reaction coordinate exceeds the activation energy, i.e., the barrier height (or the heat of reaction, if the reaction does not have a distinct transition state). The probability of this event can be calculated using the statistical approach of the RRKM theory. For the parent CH_4^+ ion, the available internal energy is the part of the excitation energy beyond the ionization threshold, which is converted to vibration energy. After dissociation, the internal energy of secondary fragments is less than the energy of the parent molecule, because of the fact that the excess energy is distributed among the product species and can be approximated as being proportional to the ratio of internal degrees of freedom of the fragment and the parent molecule. The reaction coordinate should be excluded from the total numbers of internal degrees of freedom, because the kinetic energy along the reaction coordinate is supposed to be close to the barrier's height and is already subtracted from the total internal energy. For the reaction $CH_4^+ \rightarrow CH_3^+ + H$, the available internal energy of the CH_3^+ fragment is given as

$$E_1 = (E_0 - 36.6) \times \frac{6}{8}$$

where E_0 is the initial photon energy, 6 is the number of internal degrees of freedom of the CH_3^+ fragment, and 8 is the number of degrees of freedom of the CH_4^+ ion, excluding the reaction coordinate ($9 - 1 = 8$). According to the scheme presented in Figure 7, the barrier height for the reaction $CH_3^+ \rightarrow CH_2^+ + H$ is 120.7 kcal/mol, so the minimum energy of the initial photon, which can initiate this secondary reaction, is given as

$$E_{CH_3} = 120.7 \times \left(\frac{8}{6}\right) + 36.6 = 197.5 \text{ kcal/mol}$$

If the energy of excitation exceeds this value, CH_2^+ fragments are likely to be observed. For the reaction $CH_2^+ \rightarrow CH^+ + H$,

ation, can provide sufficient internal energy to the CH_4^+ ion for its dissociation (see Figure 7). Here, we assume that ionization occurs immediately after excitation of the parent molecule by a high-power laser with energy higher than the ionization threshold, and the ion appears in the ground electronic state. Dissociation of the CH_4^+ ion in the excited $^2A_1$ state has been studied by measuring the TREPICO spectra with synchrotron radiation.[32,33] It is possible that the excited CH_4^+ ions might also be produced in an intense laser. Figure 8 and Table 1 present the geometries of the S_1, S_2, and S_3 excited states of the CH_4^+ ion, excitation energy, and "distortion energy" of these excited states, in comparison with the equilibrium geometry of

TABLE 2: Initiation Energies for the Secondary Dissociation Reactions of the CH_4^+ Ion

fragment	Initiation Energy (kcal/mol)	
	CH_4^+ dissociation	CH_4^{++} dissociation
CH_4^+ (CH_4^{++})	36.6	14.5
CH_3^+	197.5	175.4
CH_2^+	372.0	349.9
CH^+	559.0	536.9

the reaction barrier is 104.7 kcal/mol, and the initiation energy is given as

$$E_{CH_2} = 104.7 \times \left(\frac{5}{3}\right) + E_{CH_3} = 372.0 \text{ kcal/mol}$$

For the reaction $CH^+ \rightarrow C^+ + H$, the reaction barrier is 93.5 kcal/mol, and the initiation energy is given as

$$E_{CH} = 93.5 \times \left(\frac{2}{1}\right) + E_{CH_2} = 559.0 \text{ kcal/mol}$$

In the last formula, we take into account the fact that the linear CH^+ fragment has only two rotational degrees of freedom. These results are briefly presented in Table 2. However, note that the decomposition of CH^+ cannot be described by a statistical theory such as the RRKM theory.

Excited-states calculations of the neutral CH_4 molecule reveal that the first excited state of the CH_4 molecule, with geometry close to that of the CH_4^+ ion, is unstable and easily decomposes to CH_2 and H_2 fragments via a barrier of 0.3 kcal/mol. However, no distinct transition states were observed for the reaction $CH_4^+ \rightarrow CH_2^+ + H_2$. The energy of the products is greater than the energy of the initial CH_4^+ ion by 54.2 kcal/mol.

Figure 8 shows that dissociation rate constants of the parent CH_4^+ ion and its fragments can be higher than 10^{12} s^{-1} if the internal energy is larger than 100 kcal/mol. To estimate the influence of the isotope effect on the CH_4^+ dissociation, the CD_4^+, CD_3^+, and CD_2^+ dissociation rate constants are also included in Figure 6.

Figure 9 shows the branching ratios of the CH_4^+ dissociation products at three different values of available internal energies of the initial CH_4^+ ion, up to 1 ps after the ionization. The internal energy value of $E_0 = 100$ kcal/mol is sufficient for the CH_4^+ ion dissociation, but it is less than that which is necessary for the CH_3^+ ion dissociation. Therefore, we have only two lines: one descending for the CH_4^+ ion concentration, and the other rising for the CH_3^+ ion concentration. The internal energy value of $E_0 = 225$ kcal/mol (Figure 9b) is sufficient to initiate the CH_3^+ ion dissociation. In Figure 9b, the concentration of the CH_3^+ ion initially grows, but later decreases to the zero value in favor of the CH_2^+ ion production. The internal energy value of $E_0 = 460$ kcal/mol (Figure 9c) is sufficient to initiate the CH_2^+ ion dissociation. In Figure 9c, the concentration of the CH_3^+ ion grows at a time interval of ~0.02 ps and then decreases fast to the zero value. The concentration of the CH_2^+ ion also grows at a time interval of 0.1 ps, and then it decreases in favor of the CH^+ ion production. At this internal energy value, the production of C^+ is possible. However, because of the limitations of the RRKM theory, the production of C^+ is not shown in Figure 9c.

From the aforementioned discussion, we can see that the ionization and dissociation of a molecule are greatly dependent on the intensities of the intense femtosecond laser. This leads to the appearance of the behaviors of mass spectra as a function of laser intensities (see Figure 2).
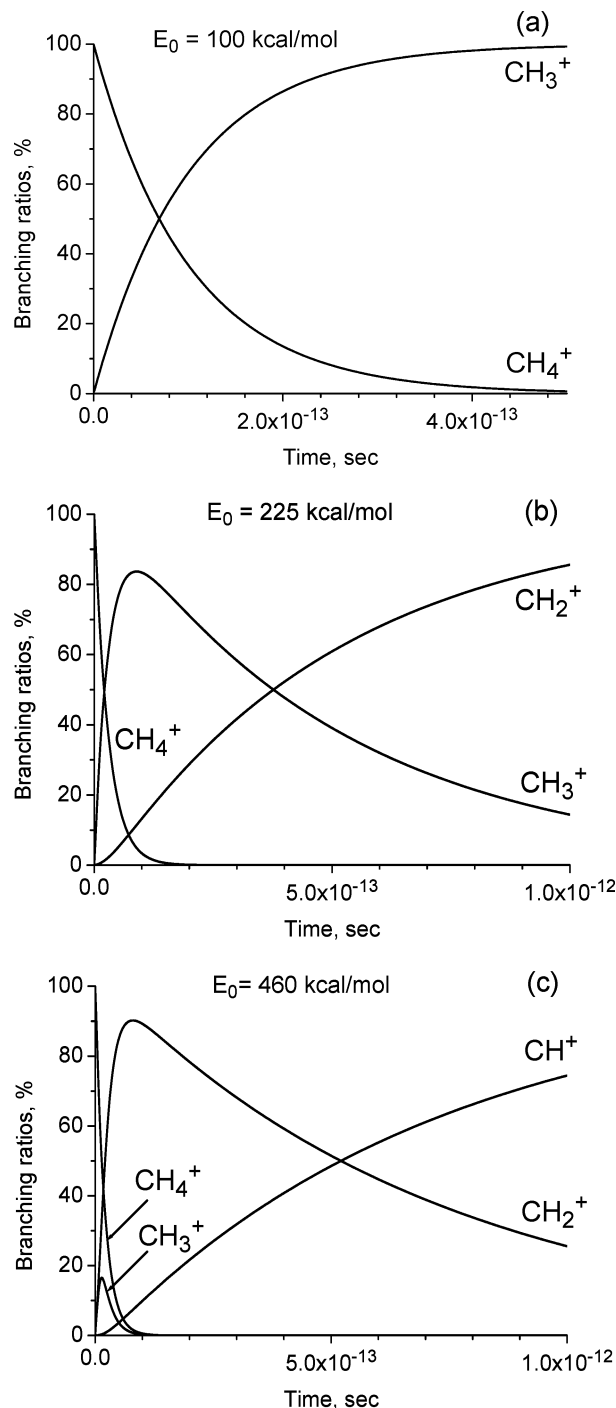
Figure 9. Branching ratios of the CH_4^+ dissociation fragments at different available internal energy (E_0) values, as a function of time.

4.2. CH_4^{++} Dissociation: Singlet State. CH_4^{++} ion has a planar square shape (Figure 10). The difference in the geometries of CH_4 and CH_4^{++} provides a large amount of internal energy for the CH_4^{++} ion, which is sufficient for the H^+ loss reaction and the H loss reaction to occur. The H^+ elimination reaction passes through transition state TS1 with a low barrier of 14.5 kcal/mol and produces the CH_3^+ ion. The next dissociation steps of this fragment have already been described in the previous section.

Because of the high intensity of laser pulses, which is necessary to produce the CH_4^{++} ion, we also can suppose that there are several molecules with an internal energy sufficient for the multistep dissociation of CH_3^+, to produce the C^+ ion
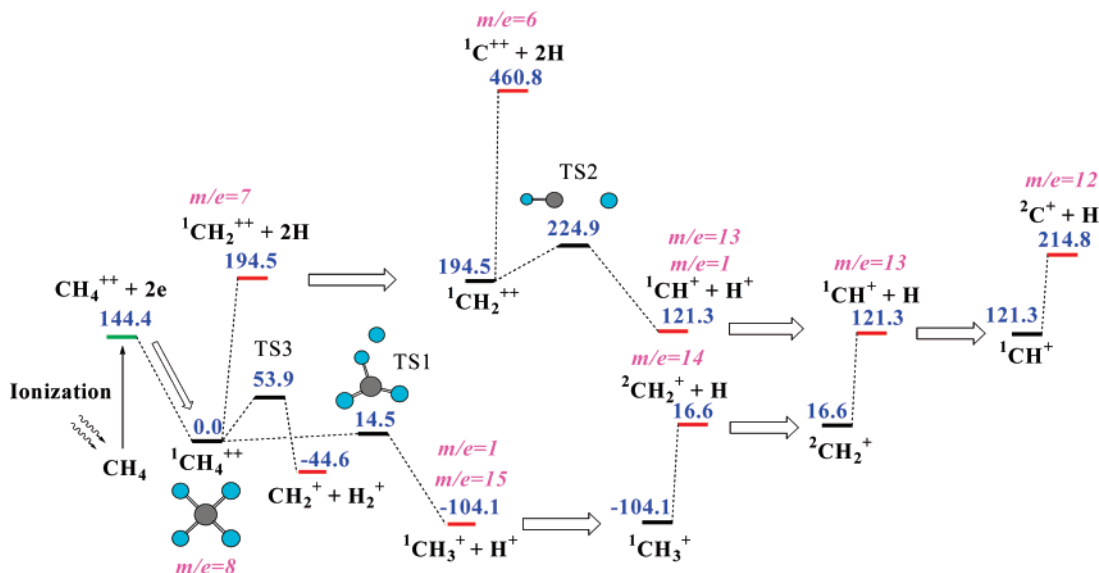
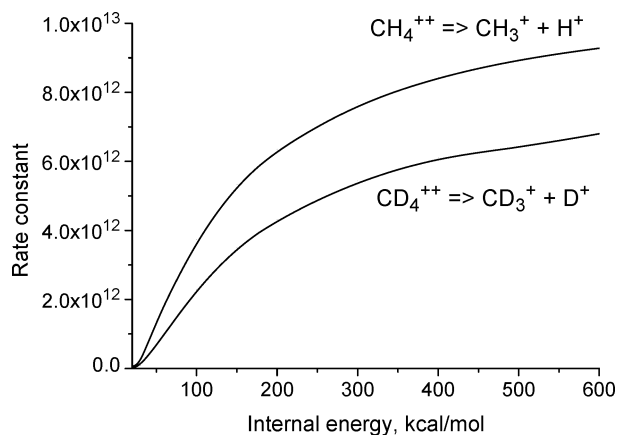**Figure 10.** CH_4^{++} dissociation. Singlet state. (All energies are given in kcal/mol.)

Figure 11. CH_4^{++} and CD_4^{++} dissociation rate constants versus the available internal energy.

eventually. Rate constants of the H elimination reaction via TS1 are given in Figure 11.

Because the $CH_4^{++} \rightarrow CH_3^+ + H^+$ reaction occurs via distinct transition state, the initiating energy for this reaction is the barrier's height at TS1, $E_{CH_4} = 14.5$ kcal/mol. The energy difference between the barrier's height and the energy of

products is converted to kinetic energies of the fragments. Using the same argument as for the CH_4^+ ion dissociation, the available internal energy of the CH_3^+ fragment is given as

$$E_1 = (E_0 - 14.5) \times \left(\frac{6}{8}\right)$$

where E_0 is the internal energy of the CH_4^{++} dication. The initiation energy for the CH_3^+ ion dissociation is given as

$$E_{CH_3} = 120.7 \times \left(\frac{8}{6}\right) + 14.5 = 175.4 \text{ kcal/mol}$$

For the reaction $CH_2^+ \rightarrow CH^+ + H$, the initiation energy is given as

$$E_{CH_2} = 104.7 \times \left(\frac{5}{3}\right) + E_{CH_3} = 349.9 \text{ kcal/mol}$$

For the reaction $CH^+ \rightarrow C^+ + H$, the initiation energy is given as

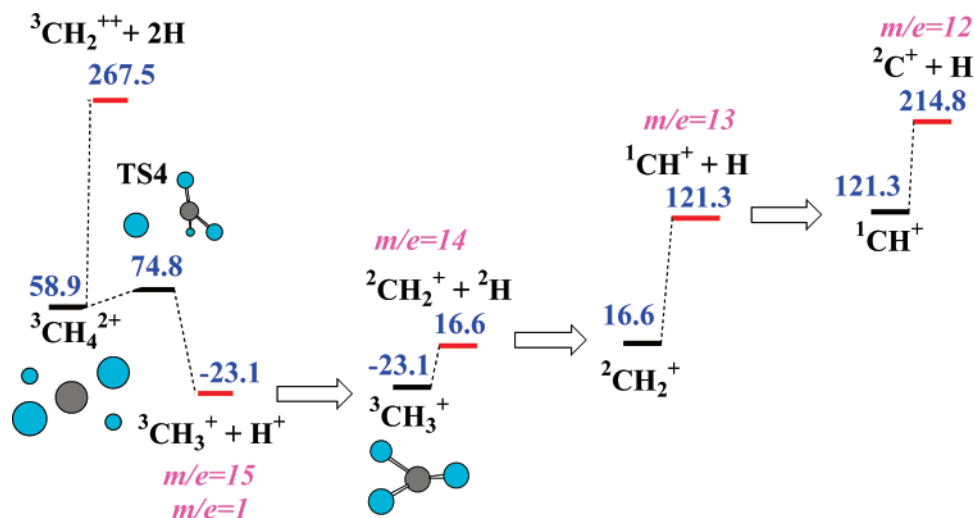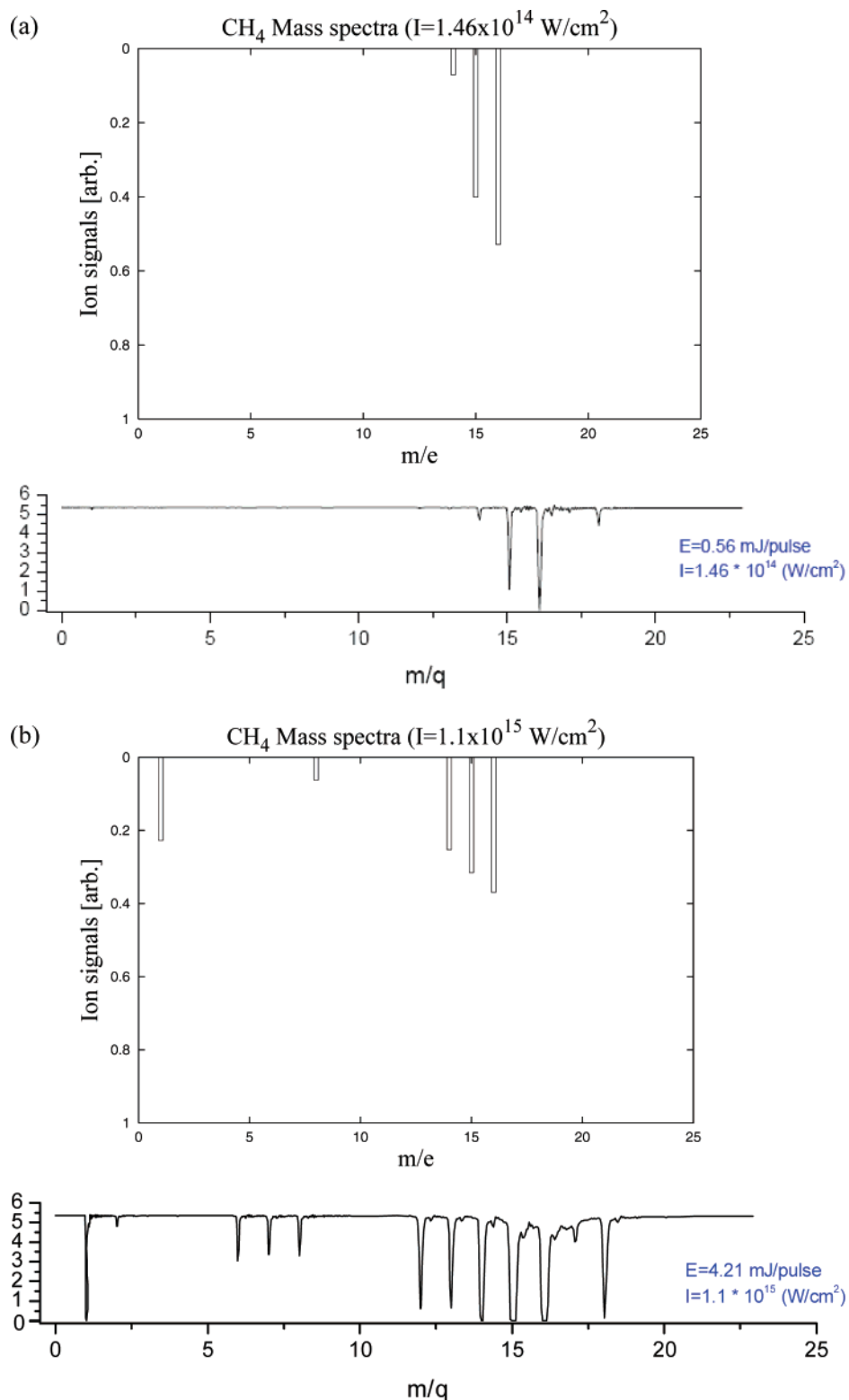$$E_{CH} = 93.5 \times \left(\frac{2}{1}\right) + E_{CH_2} = 536.9 \text{ kcal/mol}$$

Figure 12. CH_4^{++} dissociation. Triplet state. (All energies are given in kcal/mol.)

(a)

(b)

Figure 13. CH$_4$ mass spectra calculated from the RRKM theory and the generalized Keldysh theory. The peak laser intensities are chosen as (a) $I = 1.46 \times 10^{14}$ W/cm^2 and (b) $I = 1.1 \times 10^{15}$ W/cm^2, which correspond to the intensities in Figure 2. In each figure, the upper one is the theoretical result, and the lower one is the experimental result, which is shown in Figure 2. The ion signals are given in arbitrary units, whereas the sum of all mass spectra is normalized to unity.

Because the assumption that the energy difference between the barrier's height and the energy of products is converted to the kinetic energies of the fragments is very crude, and energy difference between the initiation energies of the CH$_4^+$ and CH$_4^{++}$ dissociation is small, we do not present kinetic curves for the CH$_4^{++}$ dissociation here.

The CH$_3^{++}$ dication is unstable and decomposes to produce CH$_2^+$ and H$^+$ ions. Similarly, the CH^{++} dication is unstable and decomposes to the ion pair C$^+$ + H$^+$. We had some difficulties in the calculation of the CH$_4^{++}$ → CH$_2^+$ + H$_2^+$ reaction pathway, because of the multideterminant character of the wavefunction of the CH$_4^{++}$ ion in the transition-state
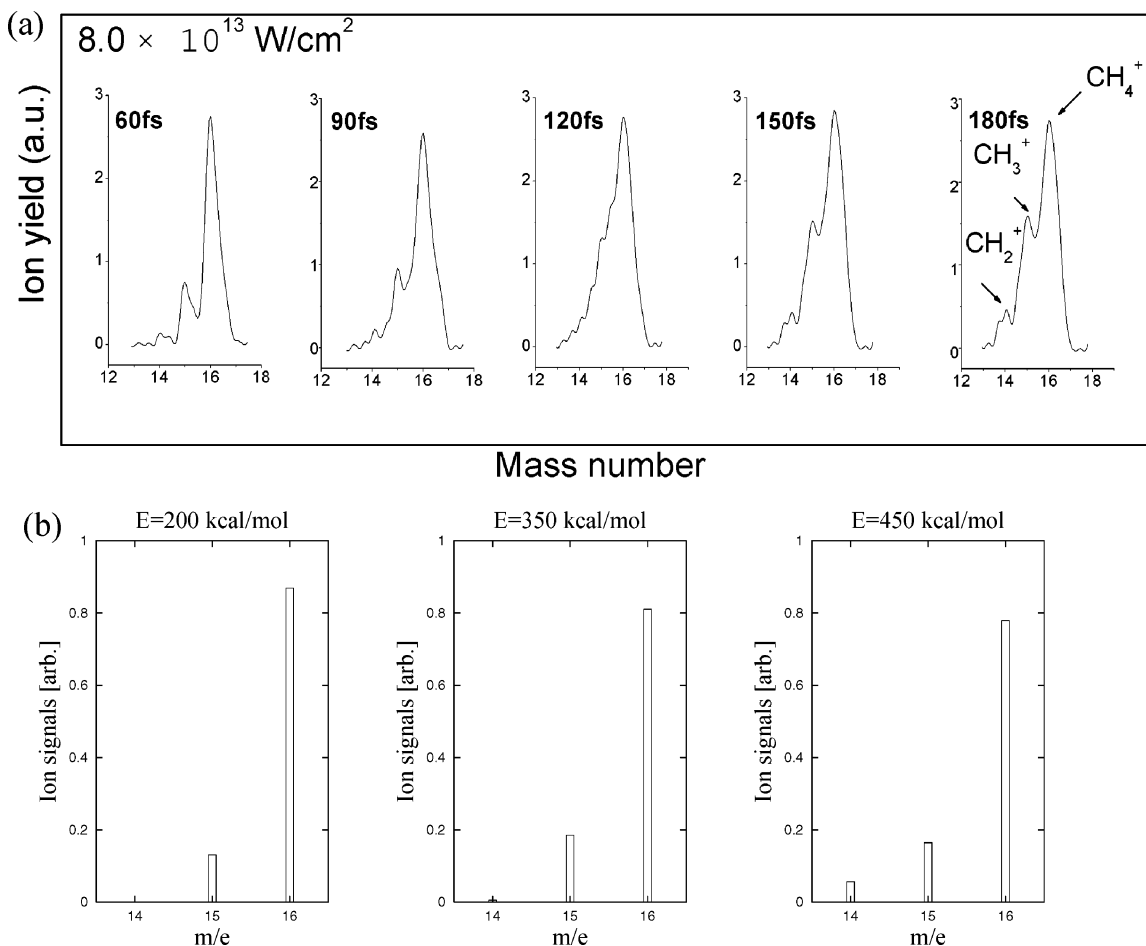
Figure 14. Plotted graphs showing (a) the TOF mass spectra of methane irradiated by an ultrafast laser with different pulse widths of 60, 90, 120, 150, and 180 fs at the same laser peak intensity of 8.0×10^{13} W/cm^2 (a CH$_4$ gas pressure of 3.3×10^{-3} Pa was maintained in the chamber, with a background pressure of 3.0×10^{-4} Pa), and (b) the mass spectra of CH$_4$ for various initiation energies.

geometry. To determine the barrier's height, we assumed that the C−H distances for both eliminating H atoms of the H$_2^+$ fragment in the transition-state geometry are the same. Therefore, the barrier's height at TS3 can be overestimated.

4.3. CH$_4^{++}$ Dissociation: Triplet State. The triplet state species of the CH$_4^{++}$ ion (see Figure 12) easily decomposes to the CH$_3^+$ + H$^+$ ion pair through a relatively low barrier at TS3. The subsequent dissociation steps of the CH$_3^+$ fragment have been already discussed previously. No pathways leading to the ^{3}CH$_2^{++}$ fragment were found. It could be supposed that if this fragment can be created, the reaction might occur in an excited state.

5. Discussion and Conclusion

In section 3, we have shown how to calculate the ionization rates and ion yields of CH$_4$ as a function of laser intensities. In section 4, we have applied the RRKM theory to evaluate the rate constants of decomposition for CH$_4^+$ and CH$_4^{++}$. In this section, we shall compute the mass spectra and compare them with those experimentally reported in section 2.

From Figure 2, we can see that if the laser intensity is $<10^{15}$ W/cm^2, only CH$_4^+$ ion and the ions resulted from the decomposition are produced; that is, the production of the CH$_4^{++}$ ion and its daughter ions are negligible. On the other hand, when the laser intensity reaches 10^{15} W/cm^2, the CH$_4^{++}$ ion and its daughter ions begin to be observable.

Qualitatively, the observed mass spectra shown in Figure 2 can be understood from Figures 7, 10, and 12. From these

figures, we can see that H$^+$ and H$_2^+$ can only be produced from CH$_4^{++}$ (in other words, only under the high laser intensity conditions). Figures 7, 10, and 12 show the mechanisms of the decomposition of CH$_4^+$ and CH$_4^{++}$ (including the singlet and triplet cases) and the initiation energy required for a particular reaction to occur.

Figure 6 shows the decomposition rate constants of CH$_4^+$ at various initiation energies; the process of the decomposition of CH$^+$ is not included, because the RRKM theory cannot be applied in this case. For comparison, the decomposition rate constants for the deuterated species are also shown in Figure 6. For demonstration, some kinetic behaviors of these reactions, under certain particular conditions, are shown in Figure 9, based on the use of the RRKM theory. The initiation energies of CH$_4^+$ and CH$_4^{++}$ are determined by the laser intensities used in the production of these ionic species (see section 3) and can be estimated from the generalized Keldysh theory for an applied laser intensity.

From the aforementioned discussion, we can see that, through the use of the theoretical results presented in sections 3 and 4, it is possible to construct mass spectra theoretically and compare the theoretical mass spectra with the experiment mass spectra shown in Figure 2. The results are shown in Figure 13; comparing Figure 13 with Figure 2, we can see that the signals of H$_2^+$, C^{+++} (or CH$_4^{++++}$), C^{++}, and CH$_2^{++}$ are missing from the theoretical spectra for $I = 1.9 \times 10^{15}$ W/cm^2 for the following reasons. The production of C^{+++} and CH$_4^{++++}$ requires higher ionization energies, such as those observed for

$CH_4^{++} \rightarrow CH_4^{+++}$ and $CH_4^{+++} \rightarrow CH_4^{++++}$, which are not available to us; the production of H_2^+ and CH_2^{++} are predicted from the theory (see Figure 10), but, because of the fact that their transition state cannot be accurately determined from our level of ab initio calculation, their production is not shown in Figure 13. The products of C^{++} and C^+ cannot be calculated from the RRKM theory, because of the smallness of their corresponding parent ions. Figure 2 shows that, when the laser intensity increases, the dissociation proceeds more, then the ion signal of C^+ will be stronger, because C^+ cannot dissociate any longer.

Recently, Wang et al.[19] reported the pulse width effect on the dissociation of CH_4^+ in the intense femtosecond laser field (see Figure 13). These mass spectra are reproduced in Figure 14; the laser pulse widths vary from 60 fs to 180 fs at the laser peak intensity of 8.0×10^{13} W/cm^2. We have computed the mass spectra using the same information discussed previously and shown them in Figure 14 for comparison. As can be seen from Figure 14, the energy dispersion must be included in the calculation to be able to reproduce the experimental spectra completely.

A similar study of high-power laser ionization and dissociation of CH_4 has also been reported by Wu et al.[20] The same theoretical analysis of mass spectra can be performed but will not be performed in this paper.

In conclusion, in this paper, we have reported the mass spectra of the high-power laser ionization and dissociation of CH_4 with intensities varying from 1×10^{14} W/cm^2 to 2×10^{15} W/cm^2 and a laser pulse width of 48 fs. In our opinion, the field-assisted dissociation of CH_4 ions can occur only if the dissociation of ions happens during the exposure of ions to the laser, because, in this case, the potential surfaces of ions can be greatly modified by the intense laser field for the dissociation to occur. If the dissociation of ions happens outside the influence of the applied laser field, then statistical theory such as the RRKM theory can be applied to calculate the observed mass spectra. This approach has been applied to analyze the experimental mass spectra. The agreement between the experimental spectra and the calculated results seems to be reasonable.

References and Notes

(1) von Koch, H. *Ark. Fys.* **1965**, *28*, 529.

(2) Powis, I. *J. Chem. Soc. Faraday Trans.* **1979**, *75* (2), 1294.

(3) Field, T. A.; Eland, J. H. D. *J. Electron Spectrosc. Relat. Phenom.* **1995**, *73*, 209.

(4) Stockbauer, R. *J. Chem. Phys.* **1973**, *58*, 3800.

(5) Dutuit, O.; Ait-Kaci, M.; Lemaire, J.; Richard-Viard, M. *Phys. Scr., T* **1994**, *31*, 223.

(6) Furuya, K.; Kimura, K.; Sakai, Y.; Takayanagi, T.; Yonekura, N. *J. Chem. Phys.* **1994**, *101*, 2720.

(7) Chin, S. L. In *Advances in Multiphoton Processes and Spectroscopy*, Vol. 16; Lin, S. H., Villaeys, A. A., Fujimura, Y., Eds.; World Scientific: Singapore, 2004; pp 249−272.

(8) Elshakre, M. E.; Gao, I. R.; Tang, X. P. *J. Chem. Phys.* **2003**, *119*, 5397.

(9) Wang, S. F.; Tang, X. P.; Gao, I. R. *J. Phys. Chem. A* **2003**, *107*, 6123.

(10) Tang, X. P.; Wang, S. F.; Elshakre, M. E. *J. Phys. Chem. A* **2003**, *107*, 13.

(11) Tang, X. P.; Becker, A.; Liu, W.; Sharifi, S. M.; Kosareva, O. G.; Kandidov, V. P.; Agostini, P.; Chin, S. L. *Appl. Phys. B* **2005**, *80*, 547−557.

(12) Tang, X. P.; Becker, A.; Liu, W.; Sharifi, M.; Kosareva, O.; Kandidov, V. P.; Agostini, P.; Chin, S. L. *Phys. Rev. A* **2005**, *71*, 045401.

(13) Assion, A.; Baumert, T.; Bergt, M.; Brixner, T.; Kiefer, B.; Seyfried, V.; Strehle, M.; Gerber, G. *Science* **1998**, *282*, 919.

(14) Levis, R. J.; Menkir, G. M.; Rabitz, H. *Science* **2001**, *292*, 709.

(15) Smith, D. J.; Ledingham, K. W. D.; Kille, H. S. *J. Phys. Chem. A* **1998**, *102*, 2519.

(16) Posthumus, J. H.; Frasinski, L. J.; Giles, A. J. *J. Phys. B* **1995**, *28*, L349.

(17) Nagaya, K.; Mishima, K.; Lu, H.-F.; Hayashi, M.; Lin, S. H. *Chem. Phys. Lett.* **2006**, *424*, 34.

(18) Nagaya, K.; Mineo, H.; Mishima, K.; Villaeys, A. A.; Hayashi, M.; Lin, S. H. *Phys. Rev. A* **2007**, *75*, 013402-1.

(19) Wang, C.; Song, D.; Liu, Y.; Kong, F. *Chin. Sci. Bull.* **2006**, *51*, 1269.

(20) Wu, Z.; Wu, C.; Liang, Q.; Wang, S.; Liu, M.; Deng, Y.; Gong, Q. *J. Chem. Phys.* **2007**, *126*, 074311.

(21) (a) Wang, S.; Tang, X.; Gao, L.; Elshakre, M. E.; Kong, F. *J. Phys. Chem. A* **2003**, *107*, 6123. (b) Mebel, A. M.; Zyubina, T. S.; Dyakov, Y. A.; Bandrauk, A. D.; Lin, S. H. *Int. J. Quantum Chem.* **2005**, *105*, 506.

(22) Mishima, K.; Hayashi, M.; Yi, J.; Chin, S.; Selzle, H. L.; Schlag, E. W. *Phys. Rev. A* **2002**, *66*, 033401.

(23) (a) Keldysh, L. V. *Sov. Phys.−JETP* **1965**, *20*, 1307. (b) Gribakin, G. F.; Kuchiev, M. Yu. *Phys. Rev. A* **1997**, *55*, 3760.

(24) Mineo, H.; Chao, S. D.; Nagaya, K.; Mishima, K.; Hayashi, M.; Lin, S. H. *Phys. Rev. A* **2007**, *75*, 027402.

(25) Mineo, H.; Chao, S. D.; Nagaya, K.; Mishima, K.; Hayashi, M.; Lin, S. H. *Chem. Phys. Lett.* **2007**, *439*, 224.

(26) Nakashima, N.; Yatsuhashi, T.; Murakami, M.; Mizoguchi, R.; Shimada, Y. In *Advances in Multi-photon Processes and Spectroscopy*, Vol. 17; Lin, S. H., Villaeys, A. A., Fujimura, Y., Eds.; World Scientific: Singapore, 2006.

(27) Frisch, M. J.; Trucks, G. W.; Schlegel, H. B.; Scuseria, G. E.; Robb, M. A.; Cheeseman, J. R.; Montgomery, Jr., J. A.; Vreven, T.; Kudin, K. N.; Burant, J. C.; Millam, J. M.; Iyengar, S. S.; Tomasi, J.; Barone, V.; Mennucci, B.; Cossi, M.; Scalmani, G.; Rega, N.; Petersson, G. A.; Nakatsuji, H.; Hada, M.; Ehara, M.; Toyota, K.; Fukuda, R.; Hasegawa, J.; Ishida, M.; Nakajima, T.; Honda, Y.; Kitao, O.; Nakai, H.; Klene, M.; Li, X.; Knox, J. E.; Hratchian, H. P.; Cross, J. B.; Adamo, C.; Jaramillo, J.; Gomperts, R. Stratmann, R. E.; Yazyev, O.; Austin, A. J.; Cammi, R.; Pomelli, C.; Ochterski, J. W.; Ayala, P. Y.; Morokuma, K.; Voth, G. A.; Salvador, P.; Dannenberg, J. J.; Zakrzewski, V. G.; Dapprich, S.; Daniels, A. D.; Strain, M. C.; Farkas, O.; Malick, D. K.; Rabuck, A. D.; Raghavachari, K.; Foresman, J. B.; Ortiz, J. V.; Cui, Q.; Baboul, A. G.; Clifford, S.; Cioslowski, J.; Stefanov, B. B.; Liu, G.; Liashenko, A.; Piskorz, P.; Komaromi, I.; Martin, R. L.; Fox, D. J.; Keith, T.; Al-Laham, M. A.; Peng, C. Y.; Nanayakkara, A.; Challacombe, M.; Gill, P. M. W.; Johnson, B.; Chen, W.; Wong, M. W.; Gonzalez, C. and Pople, J. A. *Gaussian 03*, Revision B.03; Gaussian, Inc.: Pittsburgh, PA, 2003.

(28) Eyring, H.; Lin, S. H.; Lin, S. M. *Basic Chemical Kinetics*; Wiley: New York, 1980.

(29) Robinson, P. J.; Holbrook, K. A. *Unimolecular Reactions*; Wiley: New York, 1972.

(30) Steinfeld, J. I.; Francisco, J. S.; Hase, W. L. *Chemical Kinetics and Dynamics*; Prentice Hall: Englewood Cliffs, NJ, 1999.

(31) MOLPRO is a package of ab initio programs written by H.-J. Werner and P. J. Knowles, with contributions from J. Almlöf, R. D. Amos, M. J. O. Deegan, S. T. Elbert, C. Hampel, W. Meyer, K. Peterson, R. Pitzer, A. J. Stone, P. R. Taylor, and R. Lindh.

(32) Kong, F.; Luo, Q.; Xu, H.; Sharifi, M.; Song, D.; Chin, S. L. *J. Chem. Phys.* **2006.** *125*, 133320.

(33) Gravel, J. F.; Luo, Q.; Boudreau, D.; Tang, X. P.; Chin, S. L. *Anal. Chem.* **2004**, *76*, 4799.